	Experiment title: Influence of the alloy microstructure on the residual stress field caused by the shot-peening of a nickel-based superalloy	**Experiment number**: MA-3096
Beamline: BM32	**Date of experiment**: From Sept. 23, 2016 to Sept. 28, 2017	**Date of report**: November 13, 2017
Shifts: 18	**Local contact(s)**: J.-S. Micha	*Received at ESRF:*

Names and affiliations of applicants (* indicates experimentalists):

G. Altinkurt[1,*], M. Fèvre[1,*], G. Geandier[2,*]

[1] LEM, UMR 104 CNRS-ONERA, Châtillon, France
[2] IJL, UMR 7189 CNRS-Université de Lorraine, Nancy

Report:

This work aims to improve the characterization and the understanding of stress relaxations in high temperature alloys for aero engine applications and to assess the ability of the Laue microdiffraction technique to quantify residual stresses in coarse-grained microstructures.
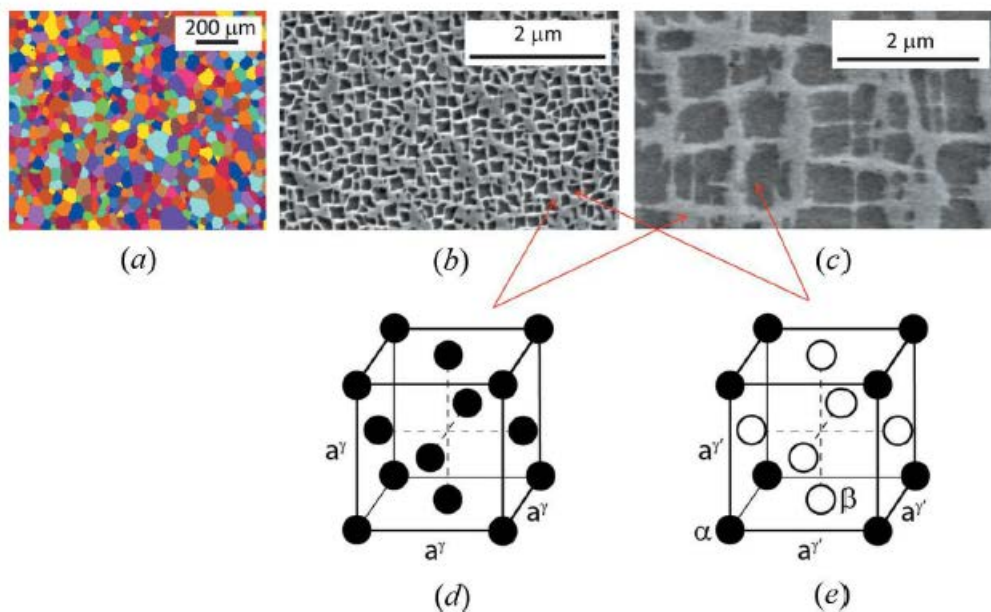

Figure 1: (a) Electron backscattered diffraction image obtained in the scanning electron microscope, revealing γ grains (random colors) and showing an average grain size of 40 μm.(b),(c) Scanning electron micrographs showing secondary γ' precipitates (dark gray) embedded into the γ matrix (light gray). (d),(e) The crystallographic structure of, respectively, the γ(A1) and the γ' (L1$_2$) phases.

Material and method: Cylindrical specimens were removed using electro discharge machining in a sector of a heat-treated high pressure turbine disk made of the N18 nickel-based superalloy produced with a powder metallurgy route at Safran Aircraft Engines. A

simplified coarse-grained microstructure (average grain size of 40 μm) with only one population of intragranular precipitates was obtained after a supersolvus solution and an ageing treatment. Two precipitates sizes were investigated: 200 nm or 2000 nm. Figure 1 represents an overview of the grain and the γ' precipitate structure. Fatigue specimens with a uniform test section (diameter of 6.2 mm) were then machined and subjected to ultrasonic shot-peening (USP) and/or fatigue conditions. Low cycle fatigue (LCF) tests were performed at 450°C with a cyclic frequency of 1 Hz and an imposed axial total strain varying in the range of 0% to 1%. These parameters correspond to a regime where plasticity is mainly accumulated during the first load cycle and a small amount of plastic deformation is then accumulated at each cycle. The tests were interrupted at approximately 25% of the lifetime (300 cycles, 1h40) to assess whether the fatigue has fully or partially relaxed the strain field caused by the shot-peening operation. After heat and mechanical treatments, the test sections were removed to have cylinders with a 10 mm height. Cross sections were then mechanically and chemically polished to remove the stresses induced by the machining operation. The Laue microdiffraction technique was used to map the strain fields and the crystalline misorientations on one of the two cross sections. To investigate the effect of the alloy microstructure and the fatigue on the strain field introduced by the shot-peening operation, four samples were characterized during this experiment (see Table 1).

Ref.	Average γ' precipitate size (nm)	Mechanical treatment
S1	2000	USP
S2,S3	200	USP
S4	200	USP+LCF

Table 1: Summary of the main characteristics of the investigated specimen. USP stands for ultrasonic shot-peening and LCF for low-cycle fatigue.

μXRD measurements were performed in the BM32 beamline at the ESRF [1]. The 5-22 keV incoming polychromatic beam was focused with Kirkpatrick-Baez mirrors to have a 0.7x0.7 μm² size on the sample surface. The diffraction patterns were collected with a circular CCD detector located 70 mm above the sample. Owing to the grain and beam sizes, Laue patterns were composed of diffraction spots originating from one or a few grains. The mapping of the sample surface was realized with a motorized *xyz* linear translation stage. The experimental geometry calibrations and the diffraction pattern analysis were performed with the LaueTools software developed by the BM32 beamline staff of the ESRF [2]. This led to the determination of the crystal orientation matrix and the unit cell parameters (b/a, c/a, α, β, γ). Owing to the fact that energy discrimination is not possible with the used CCD detector, the energy of Bragg spots is unknown and the *a* cell parameter is not determined. Assuming that the deformed unit cell has the same volume as the undeformed unit cell, the six independent components of the deviatoric strain tensor, ε^{d}_{ij} (i,j=1,2,3) can be calculated within the small transformation hypothesis in the crystal system of coordinates and then, using the crystal orientation matrix, expressed in the laboratory, sample holder and the sample coordinate. In this study, the uncertainties related to deviatoric strains were estimated to be 2×10^{-4}. To determine the *a* cell parameter and thus the full strain tensor, the energy of at least a Bragg reflection must be measured. For this purpose, a fluorescence spectra was collected using a silicon drift detector mounted upon a *yz* linear translation stage on the sample side [3]. The

simulation capabilities of the LaueTools software provided the Laue pattern on the sample side and allowed to position the energy dispersive detector in the axis of diffracted beams. The 150 eV energy resolution of the detector led to an accuracy on reflection energies E close to 5-10 eV. The corresponding uncertainty on the crystal lattice parameter a is in the $0.1-0.3 \times 10^{-3}$ nm range. Therefore, errors in the order of $0.3-0.8 \times 10^{-3}$ are obtained for the diagonal components of the full strain tensor. The unstrained cubic lattice parameters of the γ and γ' phases were measured by Wlodek et al. [4] after chemical etching in an N18 alloy. The strain calculations were performed with $a^{\gamma+\gamma'}{}_0=0.35917$ nm calculated using a Vegard's law. This value pertains to a microstructure with incoherent interfaces between the precipitates and the matrix.
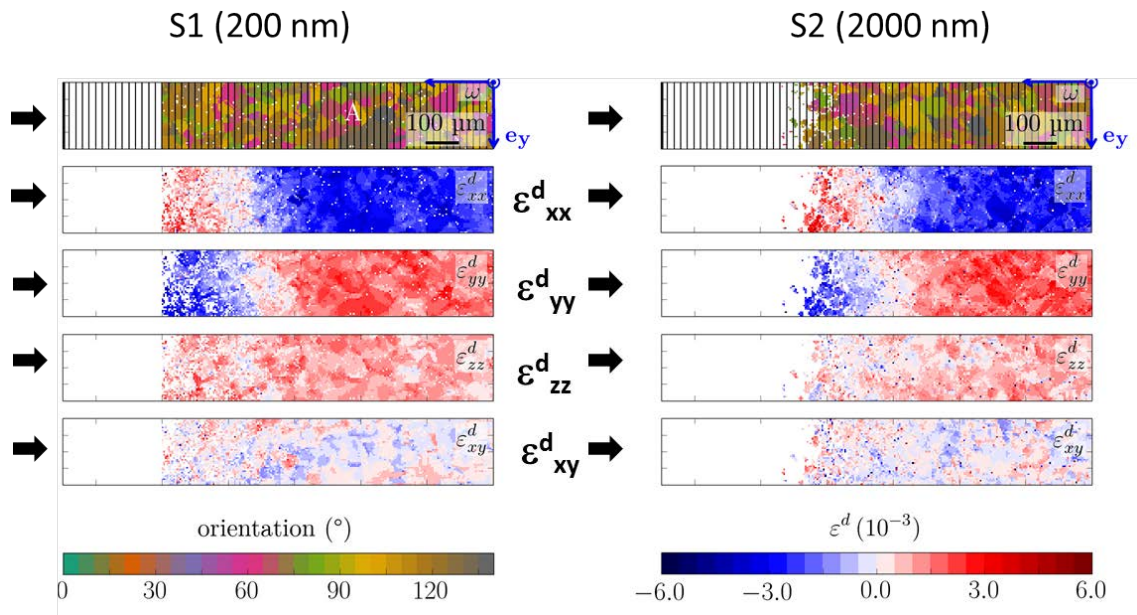
Results:

Figure 2: grain orientation and deviatoric strain maps in samples which were subjected to shot-peening. The γ' average precipitate size is 200 nm for sample S1 and 2000 nm for sample S2. The sample edge is located at the left hand side of the figures. Arrows indicate the average peening direction. Lines are isodistances from the sample edge.

Efect of the precipitate size (200 nm or 2000 nm). Fig. 2 represents the grain orientation and the deviatoric strain maps for the shot-peened samples S1 and S2. The two samples differ by the γ' precipiate size which is 200 nm or 2000 nm. Arrows located close to the sample edge correspond to the peening direction. In the white area, the crystal lattice was heterogeneously and highly deformed. The diffraction spots were thus spread out (asterism) and their intensity weakened. In this area, the measurement accuracy of the grain orientation and strains was not suffcient. The behavior of the strain fields are very similar for the two sample. For $\varepsilon^d{}_{xx}$ and $\varepsilon^d{}_{yy}$ components, strain amplitudes mainly depend on the distance from the sample edge. The main effect of the precipitate size is a shift of the strain profiles. The change of sign related to $\varepsilon^d{}_{xx}$ and $\varepsilon^d{}_{yy}$ components is indeed observed at a distance from the sample edge of 550 μm for the 200 nm precipitate size and 650 μm for the 2000 nm precipitate size.
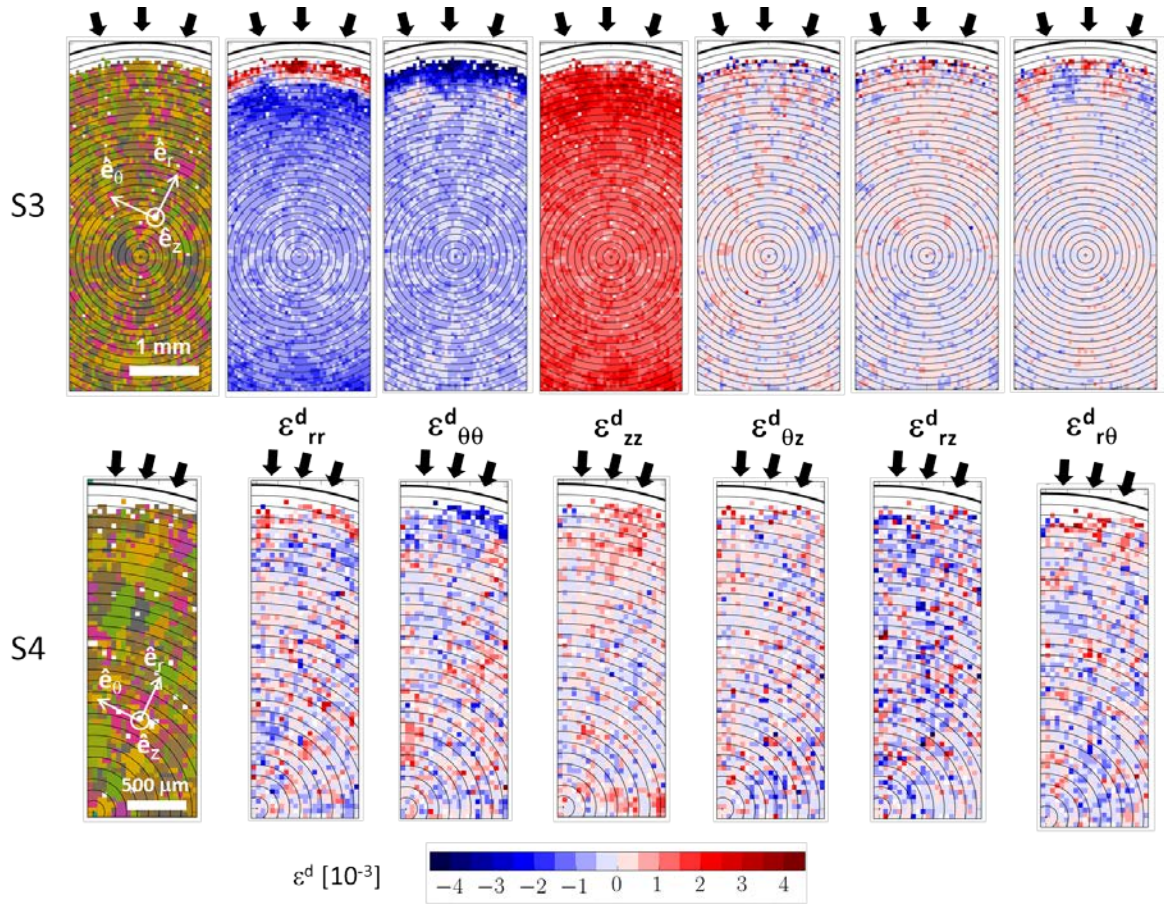
Figure 3: grain orientation and deviatoric strain maps in a sample subjected to shot-peening (S3) and in a sample subjected to shot-peening followed by 300 cycles of fatigue at 450°C (S4). The sample edge is located at the top of the figures. Arrows indicate the average peening directions. Lines are isoradius contours from the center of the sample cross section.

Effect of LCF. Measurements were realized on the cross section of the cylindrical sample whose circumference was uniformly impacted by the steel shots. The radial direction $\hat{\mathbf{e}}_r$ corresponds to the average peening direction and the axial direction $\hat{\mathbf{e}}_z$ is orientated along the surface normal of the cross section. Figure 3 represents the grain map and the maps of the six components of the deviatoric strain tensor (in units of 10^{-3}) resulting from the analysis in a 5x2 mm² mapping area for the sample S3 subjected to shot-peening only and in a 3x1 mm² mapping area for the sample S4 subjected to shot-peening and LCF. The sample edge corresponds to the last contour line at the top of maps. Arrows indicate the average shot-peening directions. The shot-peening operation strongly modified the diagonal components of the strain tensor (ε^d_{rr}, $\varepsilon^d_{\theta\theta}$, ε^d_{zz}) and weakly modified the shear components. For the diagonal components, the strain fields were modified in the entire sample cross section and mainly depended on the distance from its center. For the sample S4, only a few characteristics of the initial strain field subsisted after fatigue at 450°C: the highly deformed layer close to the sample edge and the average behavior of the 500 μm thick neighboring shell. For all components, large strain heterogeneities were observed in the rest of the maps with amplitudes in the range $\pm 2 \times 10^{-3}$ but zero on average. The underlying grain microstructure was not identifiable in strain maps because some positive and negative strains take place from one pixel to another. This means that heterogeneous intragranular deformation take place in the material.

Energy measurements were performed at different sample positions with the point detector located on the sample side. This allowed to determine the full elastic strain tensor

components. In principle, for each sample position, at least one fundamental and one superstructure reflection were searched within the translation range of the detector to determine the strain components related respectively to the average alloy ($\gamma+\gamma'$) and to the γ' phase. However, in practice, two limitations were encountered: (i) both reflections were not reachable (ii) energies of reflections were superimposed with fluorescence energies of chemical elements. For some sample positions, the energy of only one reflection was therefore determined. For the shot-peend sample (S3), the strain behavior was similar for the γ' phase (open symbols) and the average alloy (close symbols). For distances larger than 1 mm, strain amplitudes were lower than 2×10^{-3}. We observe that the behavior of the full and deviatoric components are roughly similar. They differ by less than $1-2 \times 10^{-3}$. ε_{rr} is positive and becomes negative after about 0.5 mm, whereas $\varepsilon_{\theta\theta}$ and ε_{zz} are respectively negative and positive at all distances. For the sample S4, fatigue has mostly removed the effects introduced by the shot-peening operation. All components behave in a similar manner with full strain amplitudes fluctuating between -2×10^{-3} and 2×10^{-3}. In the investigated grains, the strain of the γ' phase was very close to that of the average alloy. This suggests that residual strains in the hardened layer were also significantly relaxed for elastic equilibrium reasons.
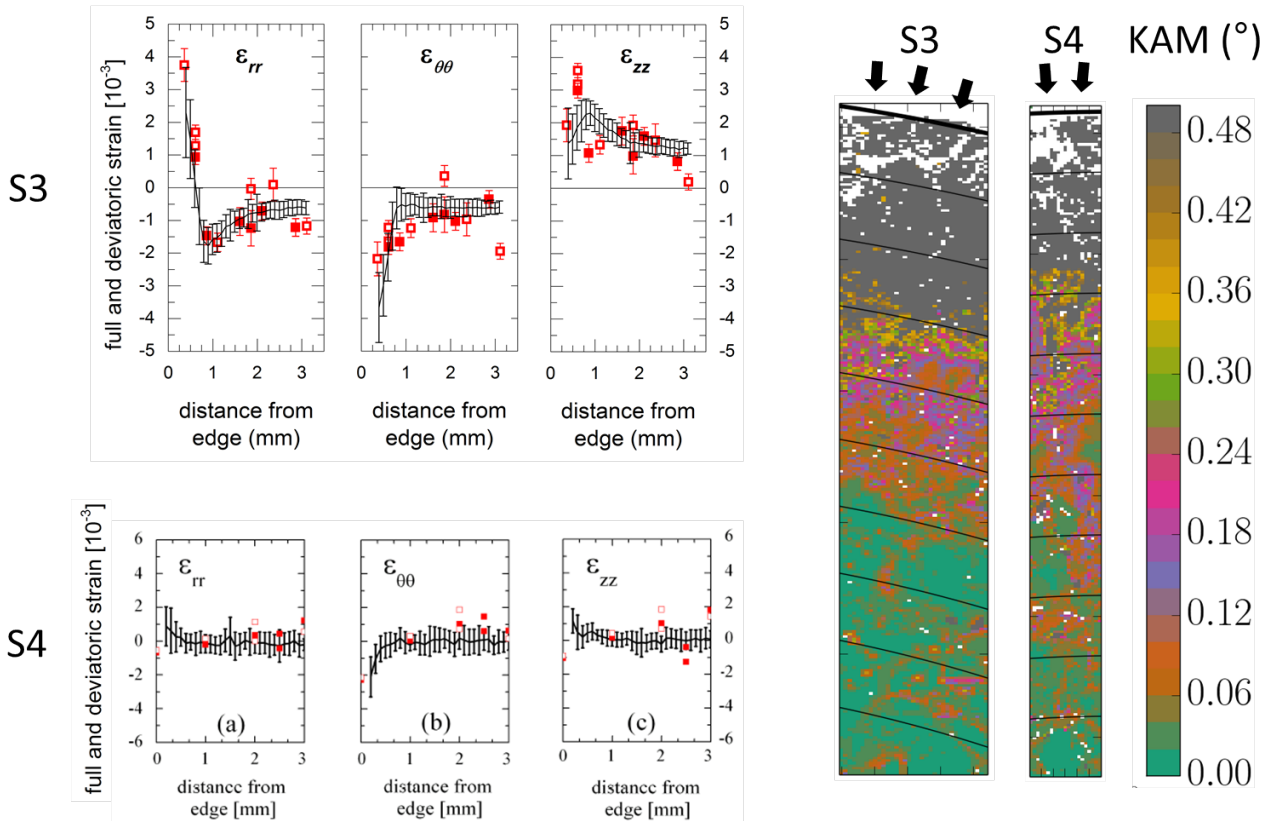

Figure 4: At the left hand side, full strain measurements (symbols) and at the right hand side KAM maps with a 0.02° step (μXRD resolution) for the shot-peened (S3) and shot-peened and fatigued (S4) states (see Tab. 1). For strain measurements, open and close symbols corresponds the average alloy and the γ' phase values obtained from the analysis of the fiundamental and the superstructure reflections of the diffraction pattern. The average value and the standard deviations obtained from the deviatoric maps of Fig. 2 are represented respectively by the line and the error bars. For the KAM maps, the sample edge is localized at the top of the figures. Arrows indicate the shot-peened edge of the samples. Isoradius contour lines are represented every 100 μm.

The kernel average misorientation (KAM) in the EBSD/SEM is used to estimate plastic strain due to surface treatments or mechanical loading conditions. Figure 4 represents KAM maps calculated from μXRD measurements with a 5 μm step size, for the shot-penned (S3)

and the shot-peened+fatigued (S4) states. The angular resolution is 0.02°, which corresponds to the accuracy of our measurements. This value is also similar to the HR-EBSD resolution. Isoradius contour lines are spaced every 100 μm. The two states are characterized by three layers: one highly deformed 300 μm thick layer close to the sample edge, a 300 μm thick layer with intragranular misorientations and in the inner part, a 400 μm thick layer where crystal misorientations were localized mostly in the vicinity of the grain boundaries. Contrary to deviatoric strain maps of Fig. 3, the map related the shot-peened state is weakly modified by the fatigue of the material.

Conclusion: The residual elastic strain field caused by the shot-peening of the N18 polycrystalline nickel-based superalloy was characterized at the grain scale and at the millimeter scale using the X-ray Laue microdiffraction technique coupled to energy measurements. The main issues that emerged from these measurements in shot-peened samples are the following. The deviatoric strain field clearly exhibits the trace of the accumulated plastic deformation in the whole sample cross-section. Strain amplitudes, which were identical for the γ and γ' phases, were so high that no sensitivity to the grain orientation was observed. The sensitivity of the Laue microdiffraction method was large enough to quantitatively characterize the crystal misorientations and the deviatoric strain redistribution after a LCF fatigue test at 450°C for the average alloy and the γ' phase. With the used method, only the KAM map can provide quantitative data in the 300 μm thick hardened layer caused by the shot-peening operation. This study also showed that the fast mapping capabilities of the Laue technique associated with the latest development of Bragg reflection energy measurements, is suitable for providing useful quantitative data for the residual stress determination in microstructures whose grain size is too large to use the $\sin^2\psi$ method or too small to use the Ortner's approach. The obtained micro- and macro-strains can be easily confronted to HR-EBSD measurements or to modeling at the grain scale (e.g. crystal plasticity or dislocation dynamics approaches) or at the mesoscopic scale (finite element based approaches). However, the obtained results suffered from the 150 eV resolution of the detector, which leads to uncertainties of 1×10^{-3} and 250 MPa on strain and stresses respectively. The small translation range of the detector and the large number of fluorescence emissions in the energy spectrum make dificult to measure the energy of a fundamental and a superstructure reflection at a fixed sample position. The use of the "Rainbow" technique should improve these two limitations. Finally, a quantitative characterization of the hardened layer was not possible because a depth resolution is required in the analysis of the Laue patterns. The differential aperture X-ray microscopy coupled to the Laue microdiffraction technique could be helpful.

References:

[1] O. Ulrich, X. Biquard, P. Bleuet, O. Geaymond, P. Gergaud, J.S. Micha, O. Robach, F. Rieutord, Rev. Sci. Instr. 82, 033909 (2011)
[2] J.S. Micha, O. Robach. Available on: http://sourceforge.net/projects/lauetools/ (2010)
[3] O. Robach, J.S. Micha, O. Ulrich, P. Gergaud, J. Appl. Cryst. 44(4), 688 (2011)
[4] S. Wlodek, M. Kelly, D. Alden, The strcuture of N18 (John Wiley & Sons, Inc., 1992), 467-471